



The Impact of Improved Spatial and Temporal Resolution of Reanalysis Data on Lagrangian Studies of the Tropical Tropopause Layer

Stephen Bourguet¹ and Marianna Linz^{1,2}

¹Harvard University Department of Earth and Planetary Sciences

²Harvard University School of Engineering and Applied Sciences

Correspondence: Stephen Bourguet (stephen_bourguet@g.harvard.edu)

Abstract. Lagrangian trajectories are frequently used to trace air parcels from the troposphere to the stratosphere through the tropical tropopause layer (TTL), and the coldest temperatures of these trajectories have been used to reconstruct water vapor variability in the lower stratosphere, where water vapor's radiative impact on Earth's surface is strongest. As such, the ability of these trajectories to accurately capture temperatures encountered by parcels in the TTL is crucial to water vapor reconstructions and calculations of water vapor's radiative forcing. A potential source of error for trajectory calculations is the resolution of the input data. Here, we explore how improving the temporal and spatial resolution of model input data impacts the temperatures measured by Lagrangian trajectories that cross the TTL during boreal winter using ERA5 reanalysis data. We do so by comparing the temperature distribution of trajectories computed with data downsampled in either space or time to those computed with ERA5's maximum resolution. We find that improvements in temporal resolution from 6 hour to 3 or 1 hour lower the cold point temperature distribution, with the mean cold point temperature decreasing from 185.9 K to 185.0 K or 184.5 K for trajectories run during boreal winters of 2010 to 2019, while improvements to vertical resolution from that of MERRA2 data (the GEOS5 model grid) to full ERA5 resolution also lower the distribution but are of secondary importance, and improvements in horizontal resolution from $1^\circ \times 1^\circ$ to $0.5^\circ \times 0.5^\circ$ or $0.25^\circ \times 0.25^\circ$ have negligible impacts. We suggest that this is caused by excess vertical dispersion near the tropopause when temporal resolution is degraded, which allows trajectories to cross the TTL without passing through the coldest regions, and by undersampling of the four-dimensional temperature field when either temporal or vertical resolution is reduced.

1 Introduction

The composition of air entering the middle atmosphere through the tropical tropopause layer (TTL) is an important control on the composition of air throughout the stratosphere. This idea was proposed by Alan Brewer in 1949 to explain his observations of a dry mid-latitude stratosphere: the coldest region that mid-latitude air may have encountered is near the tropical tropopause (Fig. 1), so the air must pass through that layer to achieve its level of dehydration (Brewer, 1949). Additional tracer observations have confirmed the existence of this overturning circulation, now known as the Brewer–Dobson Circulation (Dobson, 1956; Newell, 1963). Subsequent work has confirmed the importance of the TTL in setting the humidity of the stratosphere by

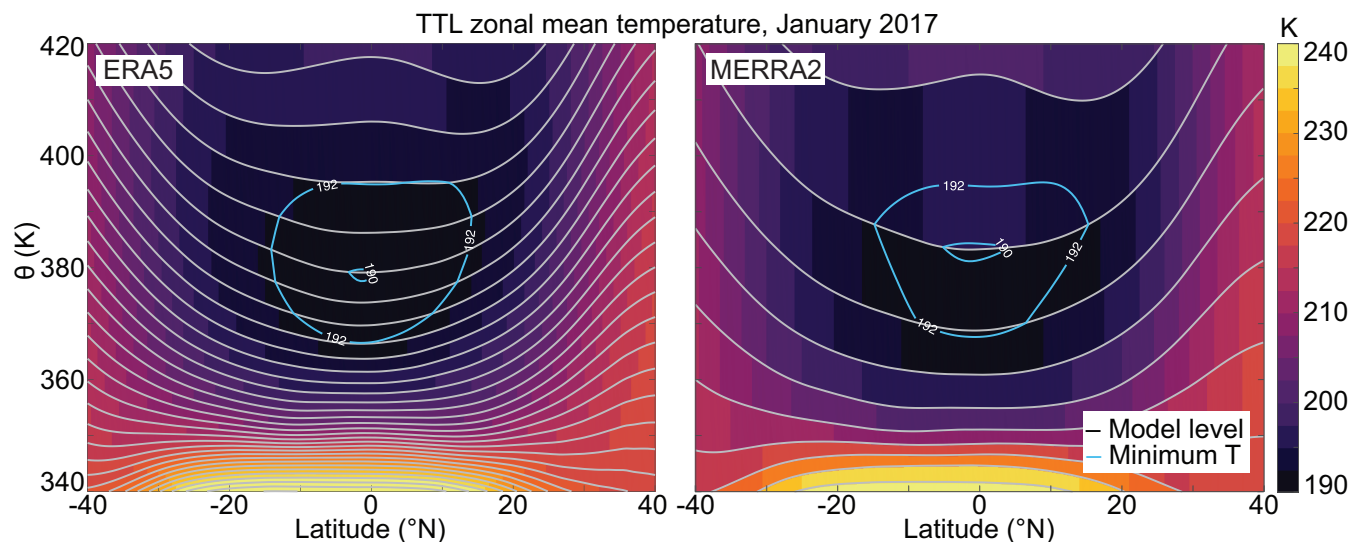


Figure 1. The January 2017 zonal mean tropical tropopause temperature for ERA5 and MERRA2 reanalysis data. Note the increased number of model layers near the coldest temperatures for the ERA5 data. A plot of the reduced resolution ERA5 data used in this paper is shown in Fig. S1.

connecting temperature variability in the TTL to water vapor variability in the lower and middle stratosphere (the “water vapor
25 tape recorder,” Mote et al. (1996); Randel and Park (2019)). Although the lower stratosphere is very dry, water vapor’s radiative
forcing is strongest in this layer, so small changes in its humidity can have a large impact on the climate (Solomon et al., 2010).

This two-dimensional description accurately describes the meridional movement of air in the stratosphere, but it does not
capture zonal variability in the circulation or in troposphere-to-stratosphere transport (TST). A seasonally varying zonal struc-
30 ture for TST was proposed by Newell and Gould-Stewart (1981) based on global 100 mb temperatures to maintain the low
humidity of the stratosphere (the “stratospheric fountain”). This framework proposes that air enters the stratosphere over the
Tropical West Pacific during boreal winter and over the Bay of Bengal and India during the boreal summer, with the majority
of the flow into the stratosphere occurring during boreal winter. Subsequent work by Holton and Gettelman (2001) countered
this hypothesis by contrasting the vertical and zonal velocities in the TTL: the vertical velocity is orders of magnitude smaller
35 than the zonal velocity, so air can circulate within the layer and encounter the “cold trap” far from where it ultimately enters
the stratosphere. The stratospheric fountain and cold trap hypotheses both introduce zonal variability in the structure of TTL
that is important for understanding the composition of the lower stratosphere. As mentioned above, the water vapor mixing
ratio at entry into the stratosphere is determined by the extent of dehydration within the TTL, and concentrations of other key
species with regional sources depend on the tropospheric origin of stratospheric air masses and their residence time within the
40 TTL (Fueglistaler et al., 2009; Randel et al., 2007). Stratospheric temperatures and circulation are also strongly impacted by
the local radiative forcing of water vapor and ozone (Maycock et al., 2011, 2013; Ming et al., 2017). Therefore, an accurate



representation of the TTL's three-dimensional structure is necessary for understanding the composition and circulation of the stratosphere.

Lagrangian trajectory models have also been used to show that the coldest temperature of trajectories that transit the TTL are predominantly encountered over the Tropical West Pacific, and that entry into the stratosphere occurs approximately 20 days later and thousands of kilometers away (Fueglistaler et al., 2004, 2005; Liu et al., 2010; Schoeberl and Dessler, 2011; Schoeberl et al., 2012, 2013). These models also show that the region controlling trajectory dehydration shifts to the Indian subcontinent and southeast Asia during boreal summer, consistent with the observations used to hypothesize the stratospheric fountain. Bowman et al. (2013) found that reanalysis products used for Lagrangian trajectory modeling available at the time of publication were deficient in temporal resolution relative to their spatial resolution. Reanalyses were available on 0.5° horizontal grids at 3 or 6 hour temporal resolution, which caused Lagrangian trajectory models to undersample the temporal variance of meteorological fields and not take advantage of the improved spatial resolution of the input data. Pisso et al. (2010) found that trajectories run on a 1° horizontal grid improved when the temporal resolution was increased from 6 hour to 3 and 1 hour, with the improvement from 6 to 3 hour being much greater than that from 3 to 1 hour. Wang et al. (2015) found that running a Lagrangian trajectory model with temperature data enhanced vertically to match GPS observations or with a correction for finer scale waves did not have a significant impact on the water vapor predicted from dehydration at the Lagrangian dry point. Therefore, improving the temporal resolution of input data for Lagrangian trajectory models may have the greatest potential to improve model performance, though improved vertical resolution may also have an effect.

Another important consideration for Lagrangian trajectory models is whether the input vertical velocities are diabatic or kinematic. Previous work has shown that kinematic trajectories are more dispersive than diabatic trajectories (Schoeberl (2004); Wohltmann and Rex (2008); Schoeberl and Dessler (2011)). Liu et al. (2010) found that this excess dispersion impacts a model's prediction of water vapor in the stratosphere based on the saturation mixing ratio of water vapor at the trajectories' Lagrangian dry point, but that this effect decreased with increased temporal resolution and with an updated reanalysis product (ERA-interim vs. ERA-40). Li et al. (2020) showed that calculations of transport to the tropopause layer by tropical cyclones using both diabatic and kinematic vertical velocities are improved when using ERA5 data in place of ERA-interim due to the improved spatial and temporal resolution of the updated reanalysis. The kinematic ERA5 trajectories in Li et al. (2020) study capture the same cold temperatures associated with convection as the diabatic trajectories do, and they represent the cyclonic air motion better than the diabatic trajectories, while the ERA-interim kinematic trajectories were not able to do so. It is therefore possible for kinematic vertical velocities provided at a high enough resolution to minimize the dispersive errors reported with older data products. This would be ideal for future studies because kinematic vertical velocities are more widely available than diabatic vertical velocities as outputs from reanalyses and models, and diabatic vertical velocities are often provided as daily or monthly means.

The stratospheric water vapor values calculated from the temperature history of the aforementioned Lagrangian trajectories studies are in good agreement with satellite observations, but it is not inconceivable that these values are right due to compensating errors. The undersampling of the temperature field due to insufficient spatial or temporal resolution is bound to produce warm (moist) biases in the cold point temperature distribution, while an underestimation of the fraction of air originating in



the troposphere due to unrealistic trajectory paths would decrease the mass of air recently undergoing dehydration and produce an additional moist bias. Therefore, improving the models' representation of how air parcels transit the TTL by increasing the temporal resolution of input data could eliminate this moist bias and decrease the water vapor concentration calculated from Lagrangian trajectory models. This would imply that an additional source of water vapor is needed to match the observed values. Previous work has suggested that ice lofting could potentially inject a significant amount of water into the lower stratosphere (Keith, 2000; Schoeberl and Dessler, 2011), as evidenced by the high observed ice water path over the central Pacific in the TTL during the 2015–2016 El Niño (Avery et al., 2017). An additional source of water vapor could also come from the ascending air's relative humidity exceeding 100% due to condensation being limited by insufficient ice nucleating particles or by cloud microphysical processes (Schoeberl et al., 2014, 2016; Ueyama et al., 2015). These hypotheses for the source of additional water vapor have flaws though: isotopic constraints have been used to suggest that ice lofting brings water vapor to the upper troposphere but not across the cold point tropopause, which means that ice lofting cannot inject significant water vapor to the lower stratosphere (Dessler et al., 2007). A similar conclusion was found using dynamic constraints by Bolot and Fueglistaler (2021), who showed that convective ice lofting supplies water up to the cold point tropopause, but that the transition to the slow ascent transport regime above that layer prevents further upward motion of significant amounts of ice. Meanwhile, the excess humidity of air entering the stratosphere may be limited by gravity waves and aging cirrus anvils, which improve the cloud dehydration efficiency by increasing the ice particle count (Schoeberl et al., 2015; Ueyama et al., 2020). Therefore, the extent to which previous Lagrangian trajectory studies of water vapor in the lower stratosphere have been biased by insufficient resolution and an inability to represent the physical processes that control lower stratospheric water vapor is an important open question.

With the release of ECMWF's updated ERA5 (Hersbach et al., 2020), we can now run Lagrangian trajectory models with 1 hour resolution and $0.25^\circ \times 0.25^\circ$ horizontal resolution on a 137 level vertical grid to analyze the improvements of kinematic trajectory models with enhanced temporal and spatial resolution. Below, we described our model setup (Section 2), show the results of our model integrations with a focus on dispersion and its impact on analysis of the TTL (Section 3), and discuss the implications of these results for future Lagrangian trajectory studies (Section 4). While improving this Lagrangian trajectory method does not directly enhance our understanding of the processes that set the the humidity of air entering the stratosphere, it does give a more accurate estimation of the extent to which processes beyond a simple cold point dehydration mechanism must be considered in calculating this value.

2 Methods

2.1 Model and data

We use ECMWF's (European Center for Medium-range Weather Forecasts) Lagrangian analysis tool LAGRANTO version 2 (Sprenger and Wernli, 2015), which has been updated from its precursor with more flexible ways to initialize and select trajectories, with ERA5 (ECMWF's latest reanalysis) input data (Hersbach et al., 2020). This data is available on a $0.25^\circ \times 0.25^\circ$ horizontal grid on 137 native model levels in 1 hour timesteps. When converted to pressure levels using a fixed surface



Timeframe	Temporal resolution	Horizontal resolution	Vertical resolution
DJF 2017	1 hour	$0.5^\circ \times 0.5^\circ$	137 levels
DJF 2017	3 hour	$0.5^\circ \times 0.5^\circ$	137 levels
DJF 2017	6 hour	$0.5^\circ \times 0.5^\circ$	137 levels
DJF 2017	1 hour	$0.25^\circ \times 0.25^\circ$	137 levels
DJF 2017	1 hour	$1.0^\circ \times 1.0^\circ$	137 levels
DJF 2017	1 hour	$0.5^\circ \times 0.5^\circ$	72 levels
DJF 2010 – 2019	1 hour	$0.5^\circ \times 0.5^\circ$	137 levels

Table 1. Summary of the LAGRANTO runs used to test resolution sensitivity. All runs are with ERA5 data (Hersbach et al., 2020), which was downloaded at 1 hour, $0.25^\circ \times 0.25^\circ$ or $0.5^\circ \times 0.5^\circ$, and 137 level resolution and subsampled or remapped using CDO tools.

pressure of 1013.25 hPa, ERA5 has 20 levels between 200 hPa and 70 hPa, which is an improvement from the 6 levels that
110 ERA-interim and other reanalyses (MERRA-2 and JRA-55) have in this range (Tegtmeier et al., 2020). LAGRANTO computes
parcel trajectories by integrating the velocity equation forward or backward through time using the three-dimensional kinematic
wind field. As mentioned above, trajectories run with kinematic vertical velocities are overly dispersive relative to those run
with diabatic heating rates, but this effect decreases with increased resolution and an improved data product (Liu et al., 2010;
Li et al., 2020). We acknowledge that this may still introduce some error in these calculations, but we show that it is minimal
115 due to the high resolution of the data (see Section 3.3.2).

By default, LAGRANTO integrates trajectories 12 times per input data timestep (e.g. every 5 minutes for 1 hour data or 30
minutes for 6 hour data). To test the influence of the integration timestep, we ran a set of integrations with 1 hour data and a
30 minute timestep and a set with 6 hour data and a 5 minute timestep. The results are nearly identical to the integrations run
with LAGRANTO's default timesteps (Fig. S2), so we concluded that integration length is of negligible importance and ran
120 trajectories with the default timestep. We obtained outputs once per hour regardless of the input data frequency, although our
results did not change when the output frequency was decreased to 6 hourly.

2.2 Lagrangian cold point analysis

We tested the performance of LAGRANTO in the TTL using a range of spatial and temporal resolutions as described in Table 1.
All data was obtained at 1 hour, $0.25^\circ \times 0.25^\circ$ or $0.5^\circ \times 0.5^\circ$, and 137 level resolution. The temporal resolution was decreased
125 by subsampling the instantaneous data every third or sixth hour (not averaging over these time periods), and the vertical and
horizontal resolution were reduced using CDO's remapping tools, remapeta and remapcon (Schulzweida, 2021). We chose to
reduce the ERA5 data to the vertical levels closest to those of MERRA2 rather than use MERRA2 data for this comparison to
prevent differences in the meteorological fields of the datasets from biasing the results.

Each set of trajectories was integrated backwards for 3 months from the end of February to the beginning of December. We
130 determined that a 3 month integration length was sufficient based on the convergence of the cold point statistics through the runs
(Fig. S3). We used a domain-filling technique that initializes a new set of trajectories between 5° S and 5° N at all longitudes



with 0.5° spacing at the end of each day for 5 consecutive days (for a total of over 75,000 trajectories per experiment) with all trajectories run to the same end time (integrations therefore last between 86 and 90 days). We also ran one integration between 15° S and 15° N and determined that expanding the trajectories beyond the deep tropics was not necessary for our analysis (Fig. S4). We found significant differences between the results from the two vertical resolutions, so we used the full vertical grid for the horizontal and temporal resolution comparisons (see Section 3.2 for vertical resolution comparison). In contrast, we found that our statistics did not significantly change when the horizontal resolution was increased from $1.0^\circ \times 1.0^\circ$ to $0.5^\circ \times 0.5^\circ$, and even less when increased to $0.25^\circ \times 0.25^\circ$, consistent with Bowman et al. (2013). Therefore, we performed the vertical and temporal resolution comparisons with $0.5^\circ \times 0.5^\circ$ horizontal resolution (see Section 3.1 for horizontal resolution comparison).

We chose boreal winter because upwelling into the stratosphere and the correlation between TTL temperatures and lower stratospheric water vapor are both strongest during this season (Rosenlof, 1995). We computed trajectories for DJF 2010 to DJF 2019 (with the year corresponding to the JF year), and found that our temporal resolution results were robust to the range of natural variability exhibited over the decade. We then performed our spatial resolution analysis with DJF 2017 data because of that year's neutral ENSO state and because the cold point statistics from that year are close to the mean statistics from the decade. The temporal resolution comparisons for the other years can be found in the Figs. S6-8.

Following the method of Fueglistaler et al. (2005), we used the trajectories that were initialized on the 400 K isentrope and traced below 340 K for our analysis of the Lagrangian cold point. For each trajectory in this subset, we found the cold point's temperature, pressure, potential temperature, and longitude. We then created distributions of their values using probability density functions, as well as the fraction of trajectories traced below 340 K at each timestep. Finally, we estimated the water vapor concentration at entry to the stratosphere using the saturation water vapor at the cold point taken from the Clausius–Clapeyron relationship assuming 100% relative humidity.

2.3 Dispersion and the tropopause transport barrier

To explore the well documented vertical dispersion of kinematic trajectories, we ran a set of 20 day reverse trajectories on a global $0.5^\circ \times 0.5^\circ$ horizontal grid on every 10 K between 310 K and 420 K during January 2017 with 1 and 6 hour temporal resolution. We then calculated the zonal mean and zonal variance (i.e. the variance across longitudes at a given latitude and height) of the trajectories' final displacement on each starting isentrope. We did not assume that any excess dispersion would be biased in either direction, so we expected that the zonal mean of the displacement would have been similar across temporal resolutions while the zonal variance would have a direct relationship with dispersion. This difference in variance should be largest near a transport barrier, where a proper representation of the flow should yield a low variance in displacement (the range of trajectory motion is limited by the barrier), while a poor representation of the barrier due to dispersion would allow trajectories to move to a greater range of displacements. Therefore, the variance of displacement should be low in the lower stratosphere, where the gradual ascent of air through the TTL and gradual descent of air at higher latitudes should limit the range of trajectory displacements. Increases in variance in this region that appear as resolution decreases indicate that excess dispersion interferes with the accurate representation of TST and/or the Brewer–Dobson circulation.

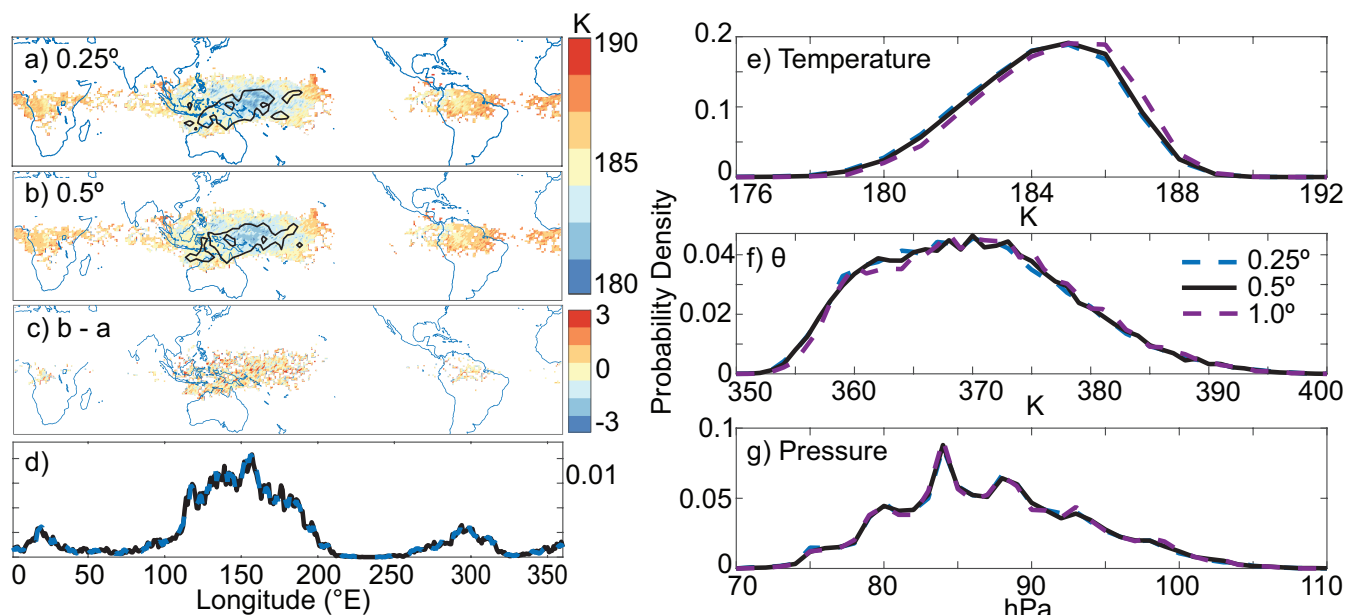


Figure 2. (a – c) Spatial distribution of the DJF 2017 trajectories’ cold point temperature, and the difference in temperature between the $0.25^\circ \times 0.25^\circ$ and $0.5^\circ \times 0.5^\circ$ trajectories. Black contours in a) and b) denote regions where the percent of trajectories crossing grid cells is greater 0.03%. d) Probability density function of the longitude of the cold point for $0.25^\circ \times 0.25^\circ$ and $0.5^\circ \times 0.5^\circ$ trajectories (which can be viewed as a weight to the temperatures in the above panels). (e – g) Probability density functions of the cold point temperature, potential temperature, and pressure for $0.25^\circ \times 0.25^\circ$, $0.5^\circ \times 0.5^\circ$, and $1.0^\circ \times 1.0^\circ$ horizontal resolution trajectories.

To look more closely at trajectory dispersion in the deep tropics, we followed the height of reverse trajectories initialized above and below the TTL transport barrier (400 K and 340 K isentropes) over the course of 90 day integrations. With increased dispersion, we expected a larger fraction of trajectories to more quickly cross the TTL, and we expected trajectories to be traced deeper into the stratosphere.

170 3 Results

3.1 Horizontal resolution

As mentioned in Section 2.1, we found that our trajectory calculations were not impacted by improving the horizontal resolution of the input data from $1.0^\circ \times 1.0^\circ$ to $0.5^\circ \times 0.5^\circ$ or $0.25^\circ \times 0.25^\circ$ for trajectories run during DJF 2017. This is evidenced in Fig. 2, which shows the cold point temperature and spatial distribution in the left column and probability density functions (PDFs) of the cold point temperature, potential temperature, and pressure in the right column. The spatial distribution of the cold points for 0.5° and 0.25° data shown in panels a and b are nearly identical (which is also shown as a PDF of cold point longitude in panel d), and the PDFs of the cold point temperature and height of 1.0° , 0.5° , and 0.25° trajectories are also not



180 significantly different. For example, 62.8%, 63.5%, and 64.1% of trajectories experience their cold point between 120 E and 200 E for the the 1.0°, 0.5°, and 0.25° trajectories, respectively. The difference between the colocated cold point temperatures shown in panel c is slightly warm biased, which is reflected by the small offset in the cold point temperature PDFs shown in panel e. (The mean cold point temperatures of the 1.0°, 0.5°, and 0.25° are 185.0 K, 184.8 K, and 184.7 K, respectively.) Similarly, the cold point pressure PDFs shown in panel g are also nearly identical for the three resolutions: the mean cold point pressures are 87.3 hPa, 87.4 hPa, and 87.4 hPa for the 1.0°, 0.5°, and 0.25° trajectories, respectively, indicating that the cold point location is not impacted by the horizontal location of the input data.

185 These results indicate that the decreased horizontal resolution does not cause trajectories to cross the TTL in regions away from the cold traps, nor does it result in undersampling of the vertical structure of the temperature field. Instead, it is likely that the slight warm bias of the lower resolution trajectories is due to undersampling of the temperature field in the horizontal, which could remove the true coldest point from the field. If a significant change in the cold point temperature was being caused by a shift in the location of the cold point, then it would be possible that the decreased sampling of the wind fields was causing the trajectories to take an erroneous path through the TTL and avoid the true cold point. But given that the shift in the cold point temperature PDF is small and that the location of the cold point does not change, the warm bias must be a function of the horizontal temperature variability, which is small on the scale being considered here. Therefore, further improvements to the horizontal resolution are unlikely to drastically change these results.

3.2 Vertical Resolution

195 The enhanced vertical resolution of the ERA5 dataset provides an opportunity to improve the accuracy of Lagrangian trajectories. As Fig. 1 shows, ERA5 has about 3 times as many vertical levels in the TTL as MERRA2, which is consistent with the ratio found by Tegtmeier et al. (2020). This enhancement is most relevant right around the cold point, which is highlighted by the blue contours in Fig. 1. The zonal mean temperatures are qualitatively similar between the two datasets otherwise, but this difference near the cold point has the potential to bias Lagrangian trajectory analyses in this region. (The downsampled ERA5 data used here is shown in Fig. S1.)

205 We have found that this difference in vertical resolution does impact Lagrangian trajectories' representation of transport across the TTL. The left column of Fig. 3 shows the temperature and spatial distributions of the cold point for trajectories run during DJF 2017 with 1 hour temporal resolution on the original ERA5 vertical grid with 137 levels (panel a), on a reduced resolution vertical grid with 72 levels (panel b), and the temperature difference (low resolution - high resolution) between the two vertical resolutions (panel c). The horizontal distribution of the cold point is similar but not identical between the two, which implies that the path taken by trajectories through the TTL is only weakly sensitive to the vertical resolution of the input winds.

210 Nonetheless, there is a 1.0 K average warm bias in the cold point temperature for the lower resolution trajectories (hence the shifted PDF in panel e), which results in a moist bias in the saturation water vapor mixing ratio of about 15%. This can be explained by a comparison of the PDFs of cold point pressure in panel g: the lower resolution trajectories have a bimodal distribution, while the higher resolution trajectories have a much smoother distribution. Absent a large change in the horizontal

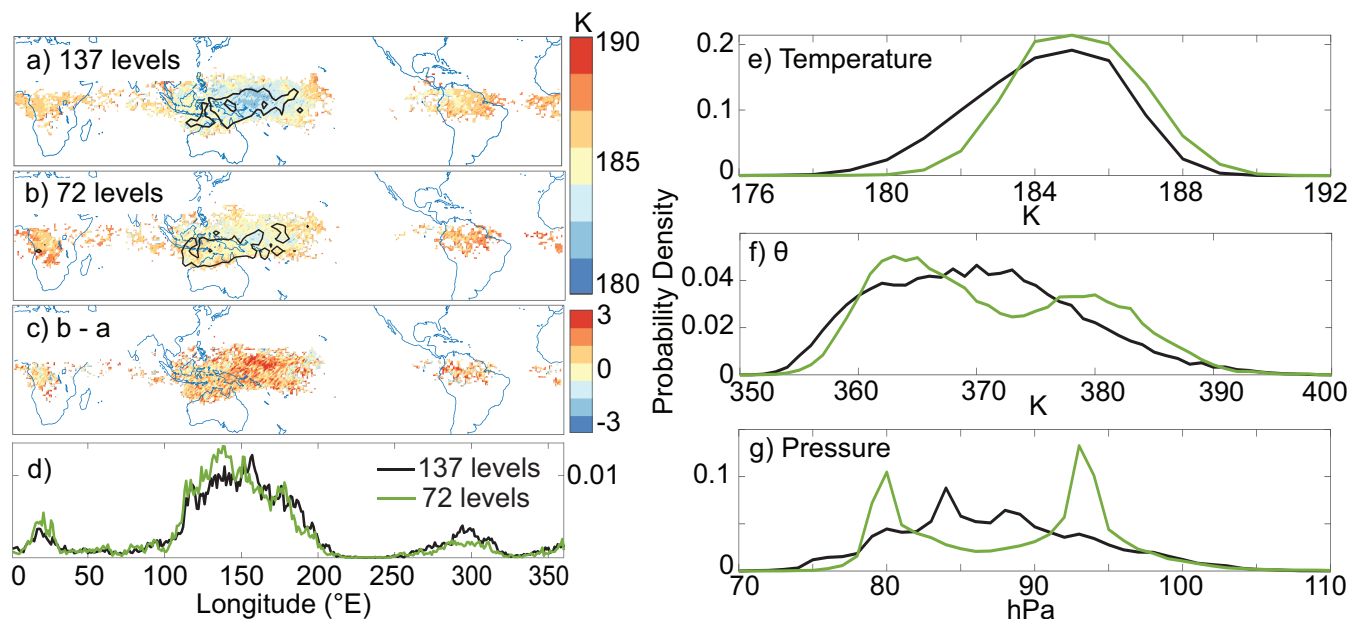


Figure 3. (a – c) Spatial distribution of the DJF 2017 trajectories’ cold point temperature for 137 and 72 level data, and the difference in temperature between the 72 and 137 vertical level trajectories. Black contours in a) and b) denote regions where the fraction of trajectories crossing grid cells is greater 0.03%. d) Probability density function of the longitude of the cold point for 137 and 72 vertical level trajectories (which can be viewed as a weight to the temperatures in the above panels). (e – g) Probability density functions of the cold point temperature, potential temperature, and pressure for 137 and 72 vertical level trajectories.

distribution of the cold point, this implies that the warm bias is caused by the trajectories undersampling the TTL temperatures. This result would not be predicted if only the zonal mean cold point temperatures of the datasets were considered: the difference between the zonal mean temperature for the high and low resolution grids is only 0.1 K. It is therefore important to consider
215 that many trajectories do not experience the cold point at the same height as the zonal mean cold point (both distributions in panel g would be unimodal if they did), and that there is zonal temperature variability throughout the TTL. In the regions where the temperature at the zonal mean cold point height is elevated, the trajectories cannot sample local temperatures that may be lower but instead are forced to jump to a vertical level with a greater change in temperature. Therefore, the lower vertical resolution grid reduces the ability of the trajectories to sample temperatures near the true cold point.

220 This contrasts Wang et al.’s (2015) finding that increased vertical resolution of temperature in a Lagrangian trajectory model improved the mean CPT by up to 0.3 K when using a wave resolving scheme and 0.2 K when matching the input data with GPS temperature observations. This difference can likely be explained by the much lower temporal resolution input data (6 hour wind and daily mean temperatures), which suggests the temporal resolution is more important than the vertical resolution.



3.3 Temporal Resolution

225 3.3.1 Cold Point Temperature

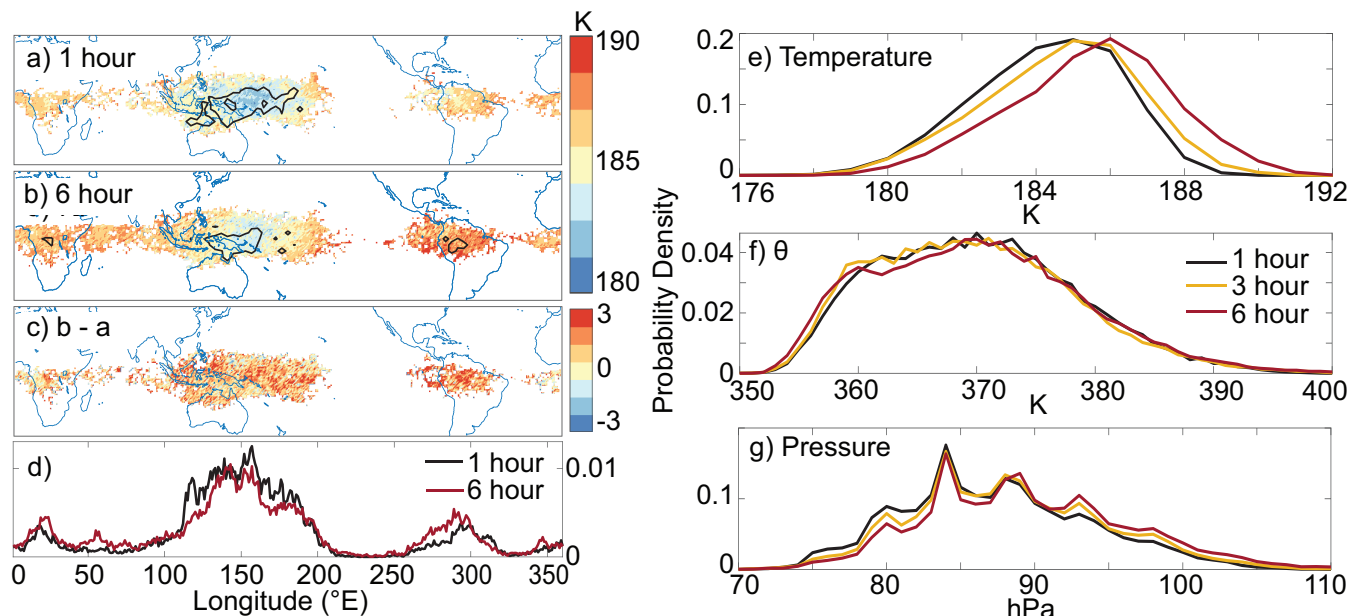


Figure 4. (a – c) Spatial distribution of the DJF 2017 trajectories’ cold point temperature for 1 hour and 6 hour, and the difference in temperature between the 6 and 1 hour trajectories. Black contours in a) and b) denote regions where the fraction of trajectories crossing grid cells is greater 0.03%. d) Probability density function of the longitude of the cold point for 1 and 6 hour trajectories (which can be viewed as a weight to the temperatures in the above panels) (e – g) Probability density functions of the cold point temperature, potential temperature, and pressure for 1, 3, and 6 hour trajectories .

Figure 4 displays the location and temperature of the cold point of DJF 2017 trajectories run with 1 hour (panel a) and 6 hour (panel b) input data, and the temperature difference (6 hour - 1 hour) for grid points where both sets of trajectories experience a cold point (panel c). This difference is almost exclusively positive and is the main source of error caused by decreased temporal resolution: the difference between the mean cold point temperature from all 6 and 1 hour trajectories is 1.4
230 K, while the difference between trajectories that experience their cold point within the same regions is 1.2 K. This accounts for about 80% of the increase in water vapor introduced by the 6 hour trajectories’ warm bias.

A secondary source of error, the zonal distribution of the cold point, can be seen by comparing the location of the cold points in panels a and b of Fig. 4 and is summarized as a probability density function of the cold point longitude in panel d. The majority of trajectories experience their coldest temperature over the western Pacific in all runs (63.5% between 120E and
235 200E for 1 hour; 60.5% for 3 hour and 53.9% for 6 hour), but the few additional cold points measured outside of this region are the warmest points seen in panel b and therefore create a warm bias with decreased temporal resolution. Previous work with



6 hour temporal resolution noted the importance of these “edge” cold points in determining the mean cold point (Schoeberl et al., 2013), but here we see that warm biases within the cold trap regions are the primary source of error. Nonetheless, the mean cold point temperature of these edge points is 3 K higher than the mean cold point temperature of the 1 hour trajectories, and this results in the remaining 20% of the moist bias introduced by decreasing the temporal resolution.

Panels e–g show PDFs of the cold point temperature and height of trajectories that transit the TTL during DJF 2017. The PDFs in panel e show the combined effects both of the warm biases discussed above: the mean cold point temperature for 1, 3, and 6 hour resolutions are 184.8, 185.2, 186.2 K, respectively. The shift in these distributions reflects the increase in the cold trap region temperatures seen in the left column of Fig. 4, while the transfer of weight from the cold tail to the warm tail of the distribution reflects the expansion of the cold point longitude distribution into warmer regions. Due to the nonlinear relationship between temperature and saturation water vapor, the water vapor calculated based on dehydration at the cold point will increase more when using the full cold point temperature distribution than it would with the mean cold point temperature (1.51 to 1.82 ppmv vs. 1.60 to 1.95 ppmv for the data shown here).

It is possible that the temperature and wind fields are both undersampled by the low resolution data. To test the impact of the temporal temperature resolution, we calculated the mean cold point temperature from the output of the 1 hour trajectories sampled every 6 hours. This would be identical to the cold point temperature calculated from the 6 hour trajectories if the temporal resolution of the temperature was the only source of the warm bias, while differences between the two would be the result of the decreased resolution of the wind field. We find that 0.5 K out of 1.4 K of the 6 hour trajectories’ warm bias can be explained by this output downsampling, leaving the remaining 0.9 K of the warm bias to the impact of the wind field’s temporal resolution.

Therefore, it is the undersampling of the wind field that creates the majority of the warm bias by altering the trajectories’ path and causing them to miss the cold point. Within the cold trap region, changes to the trajectories’ path can cause them to skip over the cold point (as seen by the shift of PDFs in panel g to higher pressures with decreased temporal resolution), while the trajectories experiencing their coldest temperatures in the edge regions are doing so by erroneously crossing the TTL away from the cold trap region.

3.3.2 Dispersion and transport across the tropopause

Figure 5 shows the zonal variance of the displacement for 1 and 6 hour trajectories initialized between 310 K and 420 K after 20 days of integration in January 2017. The variance below 350 K is similar between the two sets of trajectories, which suggests that decreasing the temporal resolution does not result in much unrealistic vertical motion beneath the tropopause. Zonal variability in vertical motion is consistent with the three-dimensional structure of tropospheric circulation (i.e. the Walker circulation, mid-latitude storm tracks), so these do not have unexpected variance. The variance increases in the TTL for both 1 and 6 hour data, and we argue that this should occur regardless of temporal resolution (though the extent to which variance increases clearly depends on temporal resolution). Tropospheric convection and lower stratospheric transport into the TTL are both zonally asymmetric and should therefore lead to a higher variance of vertical displacement for trajectories in this layer.

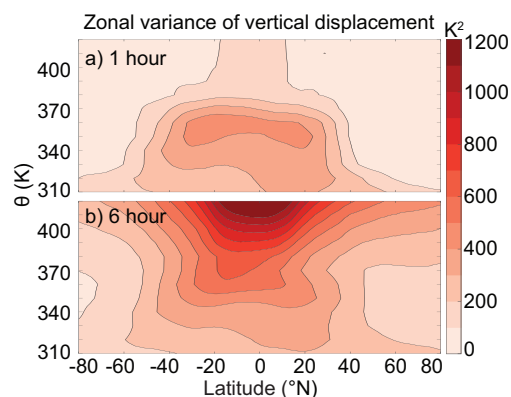


Figure 5. The zonal variance of potential temperature displacement for 1 hour and 6 hour trajectories run for 20 days between 310 K and 420 K. Contours are at every 100 K². The zonal variance of 3 hour trajectories is shown in Fig. S5.

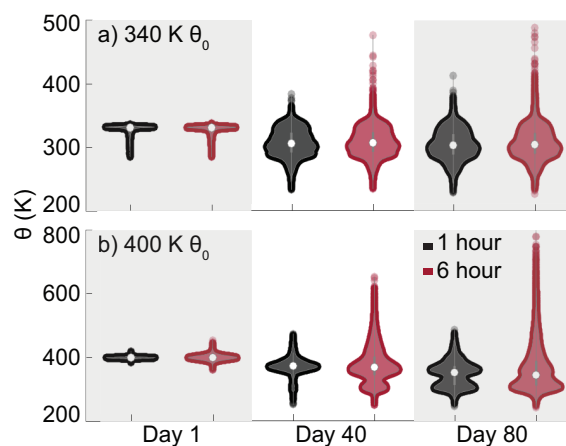


Figure 6. The distribution of trajectories' potential temperature for 1 hour (black) and 6 hour (red) runs started at 340 K and 400 K after 1, 40, and 80 days. Different y-axis are used to highlight the relevant ranges of potential temperatures.

270 The variance above 380 K diverges for the two temporal resolutions shown in Fig. 5. For the 1 hour data, the low variance in the tropics above 380 K reflects the zonal symmetry of air ascending in the upwelling branch of the BDC. For the 6 hour data, the undersampling of the wind field causes lower stratospheric trajectories to be erroneously traced either across the TTL to the troposphere or upwards into the stratosphere. We assume that the undersampling of the wind field driving the excess dispersion is random, so the increased variance should be symmetric and insensitive to the length of trajectory integration.

275 Figure 6 shows the distribution of the 1 day, 40 day, and 80 day heights for trajectories initialized at 340 K and 400 K with 1 and 6 hour input data. This confirms the impact of dispersion above and below the tropopause: the distributions of the



upper tropospheric (340 K) trajectories are nearly identical for the two temporal resolutions at all timesteps, while the lower stratospheric trajectories are impacted by the choice of resolution. The outliers at the top of the 340 K distribution for the 6 hour data after 40 and 80 days are likely driven by dispersion across the TTL, but the similarity of the distributions otherwise suggests that increased temporal resolution does not improve LAGRANTO's calculation of vertical transport in the troposphere or transport from the stratosphere to the troposphere in the deep tropics. The impact of temporal resolution on vertical transport in the lower stratosphere and TTL is revealed by the differences in the 1 and 6 hour distributions for the 400 K trajectories. After 40 days, the large majority of 1 hour trajectories are still above the TTL, while the 6 hour distribution has expanded across the TTL into the troposphere and up into the stratosphere. After 80 days, the fraction of trajectories traced to the troposphere is similar for the 1 and 6 hour resolutions, but the distribution throughout the stratosphere is substantially different.

The backwards Lagrangian trajectories studies discussed above completed integrations for at least 3 months, with some going for as long as 1 year (Fueglistaler et al., 2005; Liu et al., 2010). Increasing our integration length would not fix the issues presented here because the trajectories that have been traced upwards into the stratosphere have been committed to a physically unrealistic path. Therefore, the fraction of lower stratospheric trajectories traced back to the troposphere may ultimately be lower for the lower resolution data. Our 40 day results show that for shorter integrations, far too large of a fraction of the lower resolution trajectories are traced to the troposphere, so the low temporal resolution kinematic data is not suited for lower stratospheric studies of any length, consistent with the results of Li et al. (2020).

These results together imply that the excess dispersion resulting from insufficient temporal resolution causes lower stratospheric trajectories to be traced artificially from both above and below, thereby failing to resolve either the TTL transport barrier or the slow ascent of air in the lower stratosphere. Therefore, the origin of air in the lower stratosphere will be biased by the presence of middle stratospheric air and the underestimation of air from the troposphere when using input data with 6 hour timesteps. We remind the reader that these results are based on kinematic vertical velocities, and that, although this effect is less important when using ERA5 data, diabatic velocities are potentially better suited for studies of the stratosphere (Schoeberl, 2004; Wohltmann and Rex, 2008; Liu et al., 2010; Li et al., 2020).

300 4 Summary and discussion

Lagrangian trajectories' representation of the path of air through the TTL is degraded when the vertical and/or temporal resolution of the trajectory input data is decreased, but it is not significantly impacted by improvements to the horizontal resolution of the input data beyond $1.0^\circ \times 1.0^\circ$. We found that lowering the temporal resolution of the instantaneous input data from 1 hour to 3 or 6 hour increased the variance in displacement for trajectories initialized in the tropical lower stratosphere by an order of magnitude, though the difference between 6 and 3 hour is greater than the difference between 3 and 1 hour (see Figure 5 for the variance of 1 and 6 hour trajectories after 20 days of integration). This is consistent with Liu et al. (2010), which found kinematic trajectories with 6 hour resolution to be overly dispersive relative to diabatic trajectories run with the same temporal resolution, and Li et al. (2020), which found that diabatic and kinematic trajectories run with hourly data represented convection up to the tropopause layer better than those run with 6 hourly data (though we cannot comment on the performance



310 of trajectories run with diabatic data here). This excess dispersion causes the meteorological fields along the trajectory path to be undersampled; in particular, the distributions of Lagrangian cold point temperatures for 3 and 6 hour trajectories run during boreal winter from 2010 to 2019 have average warm biases relative to the 1 hour trajectories of 0.5 K and 1.4 K, respectively. Due to the nonlinear relationship between temperature and water vapor mixing ratio, the shifted temperature distribution for the 6 hour data results in a 26% increase in water vapor, which is greater than expected for the increase in mean CPT (positive
315 water vapor anomalies from the warm tail of the CPT distribution are of a larger magnitude than negative water vapor anomalies from the cold tail).

For reductions to the vertical resolution of the input data, we show that the warm bias in the cold point temperature is caused by undersampling of the temperature field. Trajectories are not able to observe the temperature at the cold point and are instead forced to sample temperatures at the nearest grid points; as a result the cold point height distribution of trajectories on our
320 reduced resolution grid is bimodal, while the distribution on the full resolution grid is smoother and unimodal. For reductions in temporal resolution, we show that the warm bias is caused by undersampling of both the temperature and wind fields. The majority of trajectories experience their cold points in the same “cold trap” regions regardless of temporal resolution, but there is a warm bias within these regions for the lower resolution trajectories, and the cold points erroneously measured outside of these regions by the 6 hour trajectories are 3 K warmer than those measured within. About one third of the warm bias can be
325 explained by sampling the 1 hour output every 6 hours, while the remaining two thirds can be explained by the altered path taken by the 6 hour trajectories.

The increased dispersion of trajectories resulting from decreased temporal resolution also increased the fraction of trajectories traced to the troposphere from the lower stratosphere during DJF 2010 to 2019 from 0.58 for 1 hour input data to 0.62 and 0.64 for 3 and 6 hour data, respectively. This reflects the impact of dispersion on the trajectories’ treatment of the tropopause
330 transport barrier, though the fractions may be sensitive to the length of integration. The trajectories that are erroneously traced upwards into the stratosphere are unlikely to return to the lower stratosphere or cross into the troposphere on a timescale relevant to studies of troposphere–to–stratosphere transport, so the fraction of trajectories traced to the troposphere could end up being too low for longer integrations without sufficient temporal resolution. The origin of air largely controls the composition of the lower stratosphere, so under- or overestimating the portion of air recently traced to the troposphere will result in a
335 composition that is biased by this error (i.e. too dry for too large of a fraction or too moist for too low of a fraction).

Here, we have showed that the statistics obtained from Lagrangian trajectories run across the TTL are sensitive to the temporal and vertical resolution of their input data but not horizontal resolution increases beyond 1°. Although we cannot evaluate the trajectories calculated with 1 hour data relative to the ground truth, it is clear from this work that lower stratospheric trajectories run with 3 and 6 hour data are impacted by excess dispersion in the TTL. The improvement from 6 hour to 3 hour
340 is larger than that from 3 hour to 1 hour, implying that further improvements could be small (the mean cold point temperature decreases by 0.9 K when increasing from 6 hour to 3 hour resolution and 0.5 K when increasing from 3 hour to 1 hour resolution). Similarly, input data with the full ERA5 137 level vertical grid smooths out the distribution of trajectories’ cold point heights and decreases their cold point temperature distribution, but it remains possible that additional vertical levels could further improve the trajectories’ representation of troposphere–to–stratosphere transport through the TTL. Consistent



345 with Bowman et al. (2013), we found that improvements to horizontal resolution beyond $1.0^\circ \times 1.0^\circ$ do not significantly
change the cold points observed by trajectories. Future studies of this region should consider these results when selecting
input data, although work still needs to be done to compare trajectories run with 1 hour kinematic vertical velocity and with
diabatic vertical velocity. Of course, the highest temporal and spatial resolution would minimize error if storage and computing
resources are not an issue, but reducing the horizontal resolution to $1.0^\circ \times 1.0^\circ$ will not meaningfully degrade results of
350 Lagrangian trajectory studies within this region, and the temporal resolution can also be reduced to 3 hourly if a warm cold
point temperature bias on the order of 0.5 K is acceptable.

Code and data availability. The ERA5 hourly data on native model levels from 2010 to 2019 used in this paper can be accessed through
Copernicus Climate Change Service (C3S), <https://apps.ecmwf.int/data-catalogues/era5/?class=ea>. The source code for LAGRANTO pow-
ered by ERA5 data is available upon request from Michael Sprenger. The LAGRANTO trajectories and MATLAB code to analyze trajectories
355 is archived and publicly available in Zenodo: <https://doi.org/10.5281/zenodo.6410194> (Bourguet, 2022). The colormaps were created with
the publicly available code for cbrewer (Charles, 2022), and violin plots made using publicly available code from Bechtold (2016).

Author contributions. SB: conceptualization, data curation, formal analysis, investigation, methodology, visualization, writing– original draft
preparation, review and editing. ML: conceptualization, resources, supervision, writing– review and editing

Competing interests. The authors have no competing interests to declare.

360 *Acknowledgements.* Thanks to Bill Randel for helpful conversations, and Michael Sprenger and Stephan Fueglistaler for help with calculat-
ing and interpreting trajectories.



References

- Avery, M. A., Davis, S. M., Rosenlof, K. H., Ye, H., and Dessler, A.: Large anomalies in lower stratospheric water vapour and ice during the 2015–2016 El Niño, *Nature*, 10, 405–409, 2017.
- 365 Bechtold, B.: Violin Plots for Matlab, Github Project, <https://doi.org/10.5281/zenodo.4559847>, 2016.
- Bolot, M. and Fueglistaler, S.: Tropical Water Fluxes Dominated by Deep Convection Up to Near Tropopause Levels, *Geophysical Research Letters*, 48, e2020GL091471, <https://doi.org/https://doi.org/10.1029/2020GL091471>, e2020GL091471 2020GL091471, 2021.
- Bourguet, S.: LAGRANTO resolution project data and code, <https://doi.org/10.5281/zenodo.6263451>, 2022.
- Bowman, K. P., Lin, J. C., Stohl, A., Draxler, R., Konopka, P., Andrews, A., and Brunner, D.: Input Data Requirements for Lagrangian
370 Trajectory Models, *Bulletin of the American Meteorological Society*, 94, 1051 – 1058, <https://doi.org/10.1175/BAMS-D-12-00076.1>, 2013.
- Brewer, A. W.: Evidence for a world circulation provided by the measurements of helium and water vapour distribution in the stratosphere, *Quarterly Journal of the Royal Meteorological Society*, 75, 351–363, 1949.
- Charles: cbrewer : colorbrewer schemes for Matlab, MATLAB Central File Exchange, [https://www.mathworks.com/matlabcentral/](https://www.mathworks.com/matlabcentral/fileexchange/34087-cbrewer-colorbrewer-schemes-for-matlab)
375 [fileexchange/34087-cbrewer-colorbrewer-schemes-for-matlab](https://www.mathworks.com/matlabcentral/fileexchange/34087-cbrewer-colorbrewer-schemes-for-matlab), 2022.
- Dessler, A. E., Hanisco, T. F., and Fueglistaler, S.: Effects of convective ice lofting on H₂O and HDO in the tropical tropopause layer, *Journal of Geophysical Research*, 112, <https://doi.org/10.1029/2007JD008609>, 2007.
- Dobson, G. M. B.: Origin and distribution of the polyatomic molecules in the atmosphere, *Proceedings of the Royal Society of London. Series A. Mathematical and Physical Sciences*, 236, 187–193, 1956.
- 380 Fueglistaler, S., Wernli, H., and Peter, T.: Tropical troposphere-to-stratosphere transport inferred from trajectory calculations, *Journal of Geophysical Research: Atmospheres*, 109, <https://doi.org/https://doi.org/10.1029/2003JD004069>, 2004.
- Fueglistaler, S., Bonazzola, M., Haynes, P. H., and Peter, T.: Stratospheric water vapor predicted from the Lagrangian temperature history of air entering the stratosphere in the tropics, *Journal of Geophysical Research: Atmospheres*, 110, <https://doi.org/https://doi.org/10.1029/2004JD005516>, 2005.
- 385 Fueglistaler, S., Dessler, A. E., Dunkerton, T. J., Folkins, I., Fu, Q., and Mote, P. W.: Tropical tropopause layer, *Reviews of Geophysics*, 47, 2009.
- Hersbach, H., Bell, B., Berrisford, P., Hirahara, S., Horányi, A., Muñoz-Sabater, J., Nicolas, J., Peubey, C., Radu, R., Schepers, D., Simons, A., Soci, C., Abdalla, S., Abellan, X., Balsamo, G., Bechtold, P., Biavati, G., Bidlot, J., Bonavita, M., De Chiara, G., Dahlgren, P., Dee, D., Diamantakis, M., Dragani, R., Flemming, J., Forbes, R., Fuentes, M., Geer, A., Haimberger, L., Healy, S., Hogan, R. J.,
390 Hólm, E., Janisková, M., Keeley, S., Laloyaux, P., Lopez, P., Lupu, C., Radnoti, G., de Rosnay, P., Rozum, I., Vamborg, F., Villaume, S., and Thépaut, J.-N.: The ERA5 global reanalysis, *Quarterly Journal of the Royal Meteorological Society*, 146, 1999–2049, <https://doi.org/https://doi.org/10.1002/qj.3803>, 2020.
- Holton, J. R. and Gettelman, A.: Horizontal transport and the dehydration of the stratosphere, *Geophysical Research Letters*, 28, 2799–2802, 2001.
- 395 Keith, D. W.: Stratosphere-troposphere exchange: Inferences from the isotopic composition of water vapor, *Journal of Geophysical Research: Atmospheres*, 105, 15 167–15 173, <https://doi.org/https://doi.org/10.1029/2000JD900130>, 2000.



- Li, D., Vogel, B., Müller, R., Bian, J., Günther, G., Ploeger, F., Li, Q., Zhang, J., Bai, Z., Vömel, H., and Riese, M.: Dehydration and low ozone in the tropopause layer over the Asian monsoon caused by tropical cyclones: Lagrangian transport calculations using ERA-Interim and ERA5 reanalysis data, *Atmospheric Chemistry and Physics*, 20, 4133–4152, <https://doi.org/10.5194/acp-20-4133-2020>, 2020.
- 400 Liu, Y. S., Fueglistaler, S., and Haynes, P. H.: Advection-condensation paradigm for stratospheric water vapor, *Journal of Geophysical Research: Atmospheres*, 115, <https://doi.org/10.1029/2010JD014352>, 2010.
- Maycock, A. C., Shine, K. P., and Joshi, M. M.: The temperature response to stratospheric water vapour changes, *Quarterly Journal of the Royal Meteorological Society*, 137, 1070–1082, <https://doi.org/https://doi.org/10.1002/qj.822>, 2011.
- Maycock, A. C., Joshi, M. M., Shine, K. P., and Scaife, A. A.: The Circulation Response to Idealized Changes in Stratospheric Water Vapor, 405 *Journal of Climate*, 26, 545 – 561, <https://doi.org/10.1175/JCLI-D-12-00155.1>, 2013.
- Ming, A., Maycock, A. C., Hitchcock, P., and Haynes, P.: The radiative role of ozone and water vapour in the annual temperature cycle in the tropical tropopause layer, *Atmospheric Chemistry and Physics*, 17, 5677–5701, <https://doi.org/10.5194/acp-17-5677-2017>, 2017.
- Mote, P. W., Rosenlof, K. H., McIntyre, M. E., Carr, E. S., Gille, J. C., Holton, J. R., Kinnarsley, J. S., Pumphrey, H. C., Russell III, J. M., and Waters, J. W.: An atmospheric tape recorder: The imprint of tropical tropopause temperatures on stratospheric water vapor, *Journal of* 410 *Geophysical Research: Atmospheres*, 101, 3989–4006, <https://doi.org/https://doi.org/10.1029/95JD03422>, 1996.
- Newell, R. E.: Transfer through the tropopause and within the stratosphere, *Quarterly Journal of the Royal Meteorological Society*, 89, 167–204, <https://doi.org/https://doi.org/10.1002/qj.49708938002>, 1963.
- Newell, R. E. and Gould-Stewart, S.: A Stratospheric Fountain?, *Journal of Atmospheric Sciences*, 38, 2789 – 2796, [https://doi.org/10.1175/1520-0469\(1981\)038<2789:ASF>2.0.CO;2](https://doi.org/10.1175/1520-0469(1981)038<2789:ASF>2.0.CO;2), 1981.
- 415 Pisso, I., Marécal, V., Legras, B., and Berthet, G.: Sensitivity of ensemble Lagrangian reconstructions to assimilated wind time step resolution, *Atmospheric Chemistry and Physics*, 10, 3155–3162, <https://doi.org/10.5194/acp-10-3155-2010>, 2010.
- Randel, W. J. and Park, M.: Diagnosing observed stratospheric water vapor relationships to the cold point tropical tropopause, *Journal of Geophysical Research: Atmospheres*, 124, 7018–7033, <https://doi.org/10.1029/2009GM000870>, 2019.
- Randel, W. J., Park, M., Wu, F., and Livesey, N.: A Large Annual Cycle in Ozone above the Tropical Tropopause Linked to the 420 Brewer–Dobson Circulation, *Journal of the Atmospheric Sciences*, 64, 4479 – 4488, <https://doi.org/10.1175/2007JAS2409.1>, 2007.
- Rosenlof, K. H.: Seasonal cycle of the residual mean meridional circulation in the stratosphere, *Journal of Geophysical Research: Atmospheres*, 100, 5173–5191, <https://doi.org/https://doi.org/10.1029/94JD03122>, 1995.
- Schoeberl, M., Dessler, A., and Wang, T.: Modeling upper tropospheric and lower stratospheric water vapor anomalies, *Atmospheric Chemistry and Physics*, 13, 7783–7793, 2013.
- 425 Schoeberl, M., Dessler, A., Ye, H., Wang, T., Avery, M., and Jensen, E.: The impact of gravity waves and cloud nucleation threshold on stratospheric water and tropical tropospheric cloud fraction, *Earth and Space Science*, 3, 295–305, <https://doi.org/https://doi.org/10.1002/2016EA000180>, 2016.
- Schoeberl, M. R.: Extratropical stratosphere-troposphere mass exchange, *Journal of Geophysical Research: Atmospheres*, 109, <https://doi.org/https://doi.org/10.1029/2004JD004525>, 2004.
- 430 Schoeberl, M. R. and Dessler, A. E.: Dehydration of the stratosphere, *Atmospheric Chemistry and Physics*, 11, 8433–8446, <https://doi.org/10.5194/acp-11-8433-2011>, 2011.
- Schoeberl, M. R., Dessler, A. E., and Wang, T.: Simulation of stratospheric water vapor and trends using three reanalyses, *Atmospheric Chemistry and Physics*, 12, 6475–6487, <https://doi.org/10.5194/acp-12-6475-2012>, 2012.



- Schoeberl, M. R., Dessler, A. E., Wang, T., Avery, M. A., and Jensen, E. J.: Cloud formation, convection, and stratospheric dehydration, Earth and Space Science, 1, 1–17, <https://doi.org/https://doi.org/10.1002/2014EA000014>, 2014.
- 435 Schoeberl, M. R., Jensen, E. J., and Woods, S.: Gravity waves amplify upper tropospheric dehydration by clouds, Earth and Space Science, 2, 485–500, <https://doi.org/https://doi.org/10.1002/2015EA000127>, 2015.
- Schulzweida, U.: CDO User Guide, <https://doi.org/10.5281/zenodo.5614769>, 2021.
- Solomon, S., Rosenlof, K. H., Portmann, R. W., Daniel, J. S., Davis, S. M., Sanford, T. J., and Plattner, G.-K.: Contributions of Stratospheric Water Vapor to Decadal Changes in the Rate of Global Warming, Science, 327, 1219–1223, <https://doi.org/10.1126/science.1182488>, 2010.
- 440 Sprenger, M. and Wernli, H.: The LAGRANTO Lagrangian analysis tool – version 2.0, Geoscientific Model Development, 8, 2569–2586, <https://doi.org/10.5194/gmd-8-2569-2015>, 2015.
- Tegtmeier, S., Anstey, J., Davis, S., Dragani, R., Harada, Y., Ivanciu, I., Pilch Kedzierski, R., Krüger, K., Legras, B., Long, C., Wang, J. S., Wargan, K., and Wright, J. S.: Temperature and tropopause characteristics from reanalyses data in the tropical tropopause layer, Atmospheric Chemistry and Physics, 20, 753–770, <https://doi.org/10.5194/acp-20-753-2020>, 2020.
- 445 Ueyama, R., Jensen, E. J., Pfister, L., and Kim, J.-E.: Dynamical, convective, and microphysical control on wintertime distributions of water vapor and clouds in the tropical tropopause layer, Journal of Geophysical Research: Atmospheres, 120, 10,483–10,500, <https://doi.org/https://doi.org/10.1002/2015JD023318>, 2015.
- 450 Ueyama, R., Jensen, E. J., Pfister, L., Krämer, M., Afchine, A., and Schoeberl, M.: Impact of Convectively Detained Ice Crystals on the Humidity of the Tropical Tropopause Layer in Boreal Winter, Journal of Geophysical Research: Atmospheres, 125, e2020JD032894, <https://doi.org/https://doi.org/10.1029/2020JD032894>, e2020JD032894 2020JD032894, 2020.
- Wang, T., Dessler, A. E., Schoeberl, M. R., Randel, W. J., and Kim, J.-E.: The impact of temperature vertical structure on trajectory modeling of stratospheric water vapor, Atmospheric Chemistry and Physics, 15, 3517–3526, <https://doi.org/10.5194/acp-15-3517-2015>, 2015.
- 455 Wohltmann, I. and Rex, M.: Improvement of vertical and residual velocities in pressure or hybrid sigma-pressure coordinates in analysis data in the stratosphere, Atmospheric Chemistry and Physics, 8, 265–272, <https://doi.org/10.5194/acp-8-265-2008>, 2008.